

The effect of finite-temperature and anharmonic lattice dynamics on the thermal conductivity of ZrS₂ monolayer: self-consistent phonon calculations

Abhiyan Pandit^{1,*} and Bothina Hamad^{1,2,†}

¹Physics Department, University of Arkansas, Fayetteville, AR 72701, USA

²Physics Department, The University of Jordan, Amman-11942, Jordan

Abstract

Two-dimensional (2D) ZrS₂ monolayer (ML) has emerged as a promising candidate for thermoelectric (TE) device applications due to its high TE figure of merit, which is mainly contributed by its inherently low lattice thermal conductivity. This work investigates the effect of the lattice anharmonicity driven by temperature-dependent phonon dispersions on thermal transport of ZrS₂ ML. The calculations are based on the self-consistent phonon (SCP) theory to calculate the thermodynamic parameters along with the lattice thermal conductivity. The higher-order (quartic) force constants were extracted by using an efficient compressive sensing lattice dynamics technique, which estimates the necessary data based on the emerging machine learning program as an alternative of computationally expensive density functional theory calculations. Resolve of the degeneracy and hardening of the vibrational frequencies of low-energy optical modes were predicted upon including the quartic anharmonicity. As compared to the conventional Boltzmann transport equation (BTE) approach, the lattice thermal conductivity of the optimized ZrS₂ ML unit cell within SCP + BTE approach is found to be significantly enhanced (e.g., by 21% at 300 K). This enhancement is due to the relatively lower value of phonon linewidth contributed by the anharmonic frequency renormalization included in the SCP theory. Mainly, the conventional BTE approach neglects the temperature dependence of the phonon frequencies due to the consideration of harmonic lattice dynamics and treats the normal process of three-phonon scattering incorrectly due to the use of quasi-particle lifetimes. These limitations are addressed in this work within the SCP + BTE approach, which signifies the validity and accuracy of this approach.

Keywords: Self-consistent phonon theory, Interatomic force constants, Compressive sensing technique, Lattice anharmonicity, Phonon frequency, Lattice thermal conductivity

*apandit@uark.edu,

†bothinah@uark.edu

1. Introduction

It is well known that atoms in real crystals are not fixed at rigid lattice sites but vibrating from their equilibrium position. Lattice vibrations play a vital role in describing the thermal properties of crystalline solids by means of scattering in charge transports. The density functional theory (DFT) based on the standard harmonic approximation (HA) has been routine nowadays to study the phonon dispersion relations and several thermodynamical properties [1–4]. The HA is based on the second-order derivative of the Born-Oppenheimer (BO) energy surface around the ionic equilibrium, where the atomic displacements are considered sufficiently small compared to the interatomic distances. The HA is a useful technique to describe the elastic properties, phonon spectra and lattice vibrations of a crystal at 0 K. However, the lattice anharmonicity and temperature dependences of phonon, which play a key role to explain the lattice thermal conductivity (LTC) and thermal expansion in solids, cannot be accounted within the harmonic limit. In particular, the HA fails in the crystals that have significant anharmonic effects and for the materials that are dynamically unstable at 0 K.

The consistent explanation of equilibrium properties in crystals and the limited thermal conductivity of an insulating solid requires the presence of anharmonic terms [5], which include the cubic and higher-order terms in the energy expansion. Anharmonic effects are useful properties in the finite temperature phonon dispersion relation, phonon-phonon scattering rate, phonon lifetime, shift in phonon frequencies, and so on. These parameters play an important role in the phonon transport mechanism, which determines the LTC. The density functional perturbation theory (DFPT) [6–9] or the finite-displacement method [10] have been used to treat the anharmonicity. The finite-displacement approach uses the force-displacements data to extract the cubic, quartic and higher-order terms. However, this approach becomes computationally expensive as the range of the nearest neighboring atomic interaction and the order of anharmonicity increases. The DFPT, on the other hand, considers the anharmonic self-energies as a small perturbation of the harmonic terms, which is valid only when the anharmonic terms are sufficiently smaller than the harmonic term. The high temperature phases of the ferroelectric materials with the dynamical instability [11–15] and systems with light atoms (like hydrogen) [16–19] are some examples where the perturbation theory is not applicable. Therefore, a nonperturbative approach is needed to

account the anharmonic effects for the emergent thermoelectric (TE) materials and hybrid perovskite solar cells [13,20–24].

Ab initio molecular dynamics (AIMD) simulations based approaches are generally used to account the anharmonic effects nonperturbatively [25–27]. However, the underlying problem here is in the Newtonian dynamics as its application is limited to the temperatures above Debye temperature. In addition, these AIMD based approaches are computationally expensive as well to obtain the converged phonon energies [28]. The temperature-dependent effective potential (TDEP) is one of the AIMD based approaches, which uses AIMD simulations and extracts the best possible harmonic or higher-order potential energy surfaces at finite temperatures [29]. But this approach, being an AIMD based, is limited when accounting for the zero-point vibration according to the aforementioned problem within the AIMD simulations. The self-consistent phonon (SCP) theory is another useful nonperturbative approach to include the lattice anharmonicity, which considers the quantum effect of phonons [30]. An efficient implementation of the SCP theory was developed recently [15,31], which inputs the higher-order anharmonic force constants obtained using the compressive sensing lattice dynamics (CSLD) technique [32].

Zirconium disulphide (ZrS_2) monolayer (ML) is a typical two-dimensional (2D) transition metal dichalcogenide that has been successfully synthesized [33–36]. Lowering the dimensionality and nano-structuring are reported to play major roles in suppressing the LTC that leads to an enhancement in the figure of merit (ZT) [37–41]. As compared to other similar 2D compounds, ZrS_2 ML is predicted to have a significantly low LTC upon using the conventional Boltzmann transport equation (BTE) within the relaxation time approximation (RTA), based on the harmonic phonon frequencies at 0 K [21]. In addition, the ZrS_2 ML has been predicted to have a higher ZT value of 4.5 at 800 K, which is an important result for TE efficiency enhancement and device applications. However, the inadequate understanding of the lattice anharmonicity and its effect on the phonon dispersion and lattice thermal conductivity can be misleading in revealing the actual significance of ZrS_2 ML in thermoelectrics. One may wonder how does the lattice anharmonicity and finite temperatures affect the lattice dynamics and thermodynamic properties of the ZrS_2 ML? This important issue has not been examined to date, which is the stimulus of the present work. In this work we investigate the effect of finite-temperature anharmonic phonons on the thermal transport along with the LTC of the 2D ZrS_2 ML. We used an efficient first-principles method based on the SCP theory [15,31,42,43], which calculates the temperature-dependent phonon

frequencies and LTC using the interatomic force constants (IFCs) within a supercell. The validity of this method was also well-demonstrated by carefully comparing the computed numerical results with experiments. We present brief details on the theoretical background of this work in section 2. The computational methods of the calculations are provided in section 3. The main results concerning the temperature dependence of the anharmonic phonons, lattice dynamics, thermodynamic parameters, and LTC are described in section 4. In section 5, the results are summarized by drawing final conclusions.

2. Theory

According to the BO approximation, the Hamiltonian (H) of an interacting nuclear system can be given by the sum of its kinetic energy operator (T) of ions and the potential energy (U) defined by the BO energy surface, $H = T + U$. The potential energy (U) of the system can be expressed as a Taylor expansion with respect to the atomic displacements as [15,44]:

$$U = U_0 + U_2 + U_3 + U_4 + \dots, \quad (1)$$

$$\text{where } U_n = \frac{1}{n!} \sum_{\{l,k,\mu\}} \Phi_{\mu_1, \dots, \mu_n}(l_1 k_1; \dots; l_n k_n) \times u_{\mu_1}(l_1 k_1), \dots, u_{\mu_n}(l_n k_n) \quad (2)$$

is the n th-order ($n = 2, 3, \dots, \infty$) contribution to the potential energy, $u_{\mu}(lk)$ is the atomic displacement of the atom k in the l th cell along the $\mu (= x, y, z)$ direction, and $\Phi_{\mu_1, \dots, \mu_n}(l_1 k_1; \dots; l_n k_n)$ represents the n th-order, or n -bodies, IFC, which is obtained by the n th-order derivative of the potential energy with respect to the atomic displacements. In Eq. (1) above, the linear term U_1 is neglected as the atomic forces are zero in equilibrium. In the HA, the expansion in Eq. (1) is truncated at the second order. The Hamiltonian here is transformed into Fourier space and then the harmonic phonon frequency ω is computed by constructing and diagonalizing the dynamical matrix.

The anharmonic contribution to the energy is generally expressed as a small perturbation H' added to the harmonic Hamiltonian ($H_0 = T + U_0 + U_2$) as [15,31,45,46]:

$$H = H_0 + H' \approx H_0 + U_3 + U_4, \quad (3)$$

where the higher order terms ($n > 4$) are omitted considering their contributions much smaller as compared to the third- and fourth-order terms. However, if the anharmonic terms are significant and comparable to the harmonic terms, they should be treated nonperturbatively. Using the SCP

theory [15,31,47–49], which treats the anharmonic renormalization of the phonon frequencies nonperturbatively, the Hamiltonian in Eq. (3) can be re-written as:

$$H = \mathcal{H}_0 + (H_0 - \mathcal{H}_0 + U_3 + U_4) = \mathcal{H}_0 + \mathcal{H}', \quad (4)$$

where \mathcal{H}_0 ($= \frac{1}{2} \sum_q \hbar \Omega_q \Lambda_q \Lambda_q^\dagger$) is the effective harmonic Hamiltonian associated with the displacement operator Λ_q , Ω_q is the renormalized anharmonic phonon frequency, \hbar is the reduced Planck's constant, and q is the crystal momentum vector.

The free energy of the system can be obtained as the cumulant expansion of the term \mathcal{H}' and the variational principle can be applied following the first-order SCP theory [31,43]. Then, the SCP equation can be derived as:

$$\Omega_q^2 = \omega_q^2 + 2\Omega_q I_q, \quad (5)$$

$$I_q = \sum_{q_1} \frac{\hbar \Phi(q; -q; q_1; -q_1) [2\tilde{n}_{q_1} + 1]}{4\Omega_q \Omega_{q_1}}. \quad (6)$$

Where ω_q is the harmonic phonon frequency, T is the absolute temperature, $\Phi(q; -q; q_1; -q_1)$ represent the fourth-order IFC, $\tilde{n}_{q_1} = \frac{1}{e^{\frac{\hbar \Omega_{q_1}}{k_B T}} - 1}$ is the Bose-Einstein (BE) distribution function, k_B

is the Boltzmann constant, and j is the phonon branch index for each q -point. Here, the anharmonic phonon frequencies (Ω_q) are obtained by solving above Eqs. (5) and (6) self-consistently. During the iteration process of the SCP equation, the interpolation is performed using q mesh within q_1 mesh for the inner loop.

3. Computational details

First-principles DFT calculations were performed by employing the VASP package [50,51], where the generalized gradient approximation (GGA) was used by applying the projector augmented wave method with the Perdew-Burke-Ernzerhof (PAW-PBE) functional [52]. The primitive unit cell of the 2D ZrS₂ ML was fully optimized within the self-consistent field loop convergence criteria of 10^{-6} eV. A cut-off energy of 500 eV and a Monkhorst-Pack k -mesh of $18 \times 18 \times 1$ was used including the van der Waals interactions [53]. The atomic plane and its neighboring images were separated by a sufficiently large vacuum of 22 Å in the z -direction to avoid interactions between the mirror images during the DFT calculations. The electronic band structure calculations were also performed prior the lattice dynamics calculations.

A $5 \times 5 \times 1$ supercell of ZrS₂ ML containing 75 atoms were used to extract the IFCs. To extract the harmonic IFCs, the finite-displacement approach was used. In this approach each atom was displaced from its equilibrium position by 0.01 Å including all possible nearest neighbor interactions. For the cubic IFCs, we considered up to the five-body nearest neighboring atomic interaction. The atomic forces on each of the displaced configurations were calculated, and then the cubic IFCs were extracted by using the ordinary least squares (OLS) fitting method with the harmonic IFCs as implemented in ALAMODE package [15,31,43,54]. A fitting error of 0.11 % was found here.

To estimate the IFC for the higher (quartic, or higher) order terms, the usual finite displacement method requires a large number (more than 5,000) of DFT calculations to get the atomic forces, which is computationally expensive. So, the quartic IFCs were extracted by using the CSLD technique [32], which is based on the machine learning programs as discussed and implemented in Refs. [15,31]. A $5 \times 5 \times 1$ supercell of ZrS₂ ML was initially used to conduct AIMD simulations at 300 K for 14,000 MD steps with a time step of 1.5 fs. From the trajectory of AIMD simulations, 50 equally spaced atomic configurations were extracted. All the atoms in each of the atomic configurations were then displaced by 0.1 Å in random directions. The atomic forces were then calculated for these configurations using the DFT calculations. These calculated atomic forces were then used to estimate the quartic IFCs based on the least absolute shrinkage and selection operator (LASSO) technique [55], which solves the following equation:

$$\tilde{\Phi} = \arg \min_{\Phi} \|\mathbb{A}\Phi - \mathcal{F}_{DFT}\|_2^2 + \alpha \|\Phi\|_1. \quad (7)$$

Here, L_1 regularization term is added to the least-squares method, $\Phi = [\Phi_1, \Phi_2, \dots, \Phi_M]^T$ is the vector composed of M linearly independent IFCs, \mathcal{F}_{DFT} is the vector of atomic forces, and \mathbb{A} is the matrix of atomic displacements. Moreover, α stands for the hyperparameter that controls the trade-off between the sparsity and accuracy of the model, whose optimal value was chosen from the cross-validation (CV) technique. The second order (harmonic) IFCs were fixed to the values obtained by OLS method and anharmonic terms were optimized during the LASSO regression step. The estimated quartic IFCs were used to calculate the anharmonic phonon frequency (Ω_q) after solving Eqs. (5) and (6).

The thermodynamic parameters here can be evaluated as a function of the renormalized anharmonic frequency (Ω_q). The specific heat capacity (C_v) can be calculated as:

$$C_V = \frac{k_B}{N_q} \sum_{q,j} \left(\frac{\hbar \Omega_{qj}}{2k_B T} \right)^2 \operatorname{cosech}^2 \left(\frac{\hbar \Omega_{qj}}{2k_B T} \right), \quad (8)$$

where N_q is the number of q -points.

The LTC, which is an important parameter that contributes to the TE efficiency, can be computed generally by using the BTE within RTA as [31,56]:

$$\kappa_l^{BTE} = \frac{\hbar^2}{N_q V k_B T^2} \sum_q \omega_q^2 v_q \otimes v_q n_q (n_q + 1) \tau_q, \quad (9)$$

where $v_q = \frac{\partial \omega_q}{\partial q}$, n_q , and τ_q are the group velocity, BE distribution function and quasi-particle lifetime associated with the phonon frequency ω_q , respectively; and V is the volume of the unit cell. Here as the usual BTE approach treats the anharmonic effects perturbatively, where the temperature dependence of phonon frequencies and eigenvectors are neglected. Hence, the SCP theory is used to overcome this limitation, in which the LTC is modified as [15,31]:

$$\tilde{\kappa}_l^{SCP+BTE} = \frac{\hbar^2}{N_q V k_B T^2} \sum_q \Omega_q^2 \tilde{v}_q \otimes \tilde{v}_q \tilde{n}_q (\tilde{n}_q + 1) \tilde{\tau}_q, \quad (10)$$

where $\tilde{v}_q = \frac{\partial \Omega_q}{\partial q}$ and $\tilde{n}_q = n_q(\Omega_q)$ are usual terms associated with the renormalized phonon frequency Ω_q . Here $\tilde{\tau}_q$ is the renormalized lifetime associated with the three-phonon scattering processes.

4. Results and discussions

4.1. Structural and electronic properties

The 2D ZrS₂ ML is found to crystallize in 1T structure (space group $p\bar{3}m1$) as shown in figure 1(a), where each Zr atom is octahedrally coordinated by six S atoms within the S-Zr-S sandwich layers. The unit cell of ZrS₂ ML is composed of three atoms (two Zr atoms and one S atom) with lattice parameters of $a_1 = a_2 = 3.69 \text{ \AA}$ separated by angle of 120°. This result is in agreement with the previous experimental and theoretical results [21,33,34,57–59]. The electronic structure calculations predicted an indirect band gap where the valence band maximum (VBM) and conduction band minimum (CBM) are located at Γ and M points, respectively, as shown in figure 1(b). The band gap value is found to be 1.13 eV, without including the spin-orbit interaction (SOI), which remains almost the same (1.14 eV) upon including the SOI, see figure 1(b). These results are in agreement with previous studies [21,58,60,61]. The Brillouin zone with the selected high symmetry points for the electronic band structure calculation is shown in figure 1(c).

4.2. Anharmonic force constants from the compressive sensing technique

While the cubic terms are needed to perform the BTE calculations, the harmonic and quartic IFCs are necessary inputs to conduct the SCP calculations. The aforementioned LASSO technique was adopted to estimate the quartic IFCs, where the 50 displacement-force data sets obtained using AIMD are used. The predictive accuracy of LASSO regression was tested beforehand by using a four-fold cross-validation (CV) technique. The results of the CV are shown in figure 2, where figure 2(a) represents the relative error of the atomic forces, defined as a square root of $\|\mathbb{A}\tilde{\Phi} - \mathcal{F}_{DFT}\|_2^2 / \|\mathcal{F}_{DFT}\|_2^2$, as a function of the hyperparameter α . As the value of α decreases, the CV error decreases and reaches its minimum value at $\alpha = 4.96 \times 10^{-6}$ as indicated by the dotted vertical line in the figure. This value of α was chosen for the estimation of quartic IFCs because it is expected to give an accurate prediction for the data sets. With the chosen α value, we obtained a total of 9134 non-zero quartic IFCs as shown in figure 2(b), which represents about 55% of the total number of quartic IFCs with the rest of the physically irrelevant IFCs driven to be exactly zero.

4.3. Self-consistent phonons at finite temperature

Phonons are the vibrations resulting from the thermal energy of atoms or molecules within a system. The phonon dispersion curves and density of states (DOS) of ZrS₂ ML within the HA and SCP approach are shown in figure 3. Sufficiently converged anharmonic phonon frequencies (Ω_q) were found with a $5 \times 5 \times 1$ q -grid points with respect to the intermediate $10 \times 10 \times 2$ q_I -grid points. The non-analytic correction was included by employing the Born effective charges and dielectric constants during SCP calculations. As the ZrS₂ unit cell has 3 atoms, there are a total of 9 phonon modes (3 acoustic and 6 optical), see figure 3(a). The lowest 3 phonon modes represent the acoustic modes, which are composed of in-plane longitudinal acoustic (LA), in-plane transverse acoustic (TA) modes, and out-of-plane flexural acoustic (ZA) mode. While LA and TA modes have a linear behavior near the Γ point, the ZA mode exhibits a quadratic behavior, which is due to the 2D nature ML structure [37,62]. This behavior is consistent with the results obtained for other two-dimensional materials such as graphene[4,63–65], boron nitride [66,67], silicene [68], InX (Sn, Se, and Te)[69], and MoSe₂ [70]. The phonon frequencies of low-energy optical modes of ZrS₂ ML are found to increase within the SCP approach, which is due to the included

quartic IFCs as shown in Eq. (5). The harmonic phonon frequency of the lower optical mode at Γ point is 145.36 cm^{-1} , which increases to 152.57 cm^{-1} by including the quartic anharmonicity within the SCP approach at 0 K. The frequency further increases to 162.55 cm^{-1} at 300 K temperature due to the temperature dependent term I_q within the SCP calculations (see Eqs. (5) and (6)). The degeneracy of the optical modes 4 and 5 at the Γ point in the case of the harmonic phonon spectra is broken by the inclusion of the quartic anharmonicity within the SCP method, where the frequency of the optical mode 5 increases as seen in figure 3(a) with the corresponding phonon frequencies provided in table 1. This resolve of the degeneracy and hardening of the optical modes within SCP approach highlights the particular importance of the lattice anharmonicity for ZrS_2 , which is expected to affect the LTC later. The phonon DOS as a function of vibrational frequency are depicted in figure 3(b), where the higher peaks in the phonon DOS are found at the frequency region beyond 200 cm^{-1} . This can be attributed to the fact that the number of the lighter S atom, which contributes to the higher frequency, is double than that of the heavier Zr atom in the ZrS_2 ML unit cell.

4.4. Thermodynamic parameters

The specific heat capacity (C_v) is a crucial thermodynamic quantity, which directly contributes to the LTC (κ_l) as $\kappa_l \propto C_v$. The calculated C_v as a function of temperature obtained within the SCP theory is shown in figure 4(a). The low values of C_v at temperatures below 400 K indicate smaller contributions to LTC at low temperatures. The value of C_v is found to increase as a function of the temperature until it converges to the classical limit of Dulong and Petit at higher temperatures. The mean-square displacement (MSD) is an important quantity that measures the deviation of atoms with respect to the equilibrium position in a system. The average MSD tensor of atom k is computed as:

$$\langle u_{\mu}^2(k) \rangle = \frac{\hbar}{M_k N_q} \sum_{q,j} \frac{1}{\Omega_{qj}} |e_{\mu}(k; q_j)|^2 (\tilde{n}_{qj} + \frac{1}{2}), \quad (11)$$

where $e_{\mu}(k; q_j)$ is the corresponding atomic polarization.

There is an increase in the MSDs upon increasing the temperature, which is ascribed to the increased heating effect at higher temperatures, see figure 4(b). The increase in MSDs of thermal vibrations at higher temperature contributes to reduce the thermal transport. The calculated MSDs of S atoms are found to be higher than those of Zr atoms because of the higher atomic mass of Zr

atoms and the inverse relation between atomic displacement and mass, see Eq. (11). This phenomena becomes more pronounced as the temperature increases. The total vibrational free energy is given by the sum of the free energy within the quasi-harmonic approximation (QHA) and the SCP correction term due to the anharmonicity within SCP method ($E_{\text{Total}} = E_{\text{QHA}} + E_{\text{SCP}}$). Although there is a negligible effect of SCP correction to the free energy within QHA at lower temperatures, the effect becomes more pronounced as the temperature increases as shown in figure 4(c). For instance, the SCP correction energy of -2.2 meV at 300 K decreases to -7.8 meV at 700 K. This decrease in total energy using the SCP correction indicates that the system is more stabilized by including the quartic anharmonicity. This fact also clearly highlights the importance of the anharmonic frequency renormalization on the thermal properties.

The phonon mode-dependent Grüneisen parameter (γ_{qj}) is another important dimensionless quantity that measures the anharmonic nature of the structure. This parameter is evaluated as the change of phonon frequency (ω_{qj} or Ω_q) with respect to the change in volume (V): $\gamma_{qj} = -\frac{\partial(\log \omega_{qj})}{\partial(\log V)}$ by using the cubic IFCs. A positive value of γ_{qj} indicates a decrease in the frequency of the phonon mode q,j with the increase of volume. The calculated γ_{qj} of ZrS₂ ML as a function of the phonon frequency is shown in figure 5(a), where the trend of change in γ_{qj} values for both the SCP and harmonic lattice dynamics is found to be similar. The larger negative value of γ_{qj} in the low frequency region (acoustic phonon modes) changes to small positive values at higher frequencies. This suggests larger phonon anharmonicity in the case of acoustic phonon modes. This nature closely affects the LTC via phonon life time (τ) as $\tau_{qj}^{-1} \propto \gamma_{qj}^2$ according to the continuum theory [71,72].

The cumulative phonon group velocities (v_g) of ZrS₂ ML as a function of the phonon frequency is illustrated in figure 5(b). On average, group velocities of the acoustic phonon modes are found to be higher than those of the optical phonons. The average group velocities of the acoustic and optical phonons within the harmonic (SCP) lattice dynamics are 1.84 kms⁻¹ (1.83 kms⁻¹) and 1.1 kms⁻¹ (1.05 kms⁻¹), respectively. Hence, following the relation $\kappa_l \propto v_g$, the contribution of the acoustic phonon modes to the LTC should be larger than that of optical modes.

The phonon lifetime (τ) is another significant quantity that is related to the LTC as $\kappa_l \propto \tau$ (see Eqs. (9) and (10)). It is calculated from the imaginary part of the anharmonic self-energy ($\sum_q(\omega_q)$) as $\tau_{q,anh}^{-1} = 2\Gamma_q^{anh} = 2Im \sum_q(\omega_q)$ [15,31,43], where Γ_q^{anh} is the phonon linewidth.

Figure 5(c) shows the calculated τ of ZrS₂ ML at 300 K as a function of the phonon vibrational frequency by using the harmonic and SCP lattice dynamics, where the harmonic phonon frequency (ω_q) is replaced by renormalized phonon frequency (Ω_q) for the SCP lattice dynamics. The longer phonon lifetime is found in the low frequency range (acoustic modes) due to the low phonon-phonon scattering rate. This means the low frequency phonon modes have the major contribution to transport most of the heat in ZrS₂ ML, and consequently, a significant contribution to the LTC. As the obtained quasi-particle τ values by harmonic phonons are used in usual BTE approach, where the normal process of three-phonon scattering is incorrectly treated—this would result in $\kappa_l^{BTE} < \kappa_l^{actual}$ [31] as a consequence. The average value of τ using the SCP approach (2.24 ps) is higher than that of the harmonic phonons (1.59 ps) used in BTE approach, which is ascribed to the three-phonon scattering processes included within the SCP lattice dynamics.

4.5. Lattice thermal conductivity

The LTC (κ_l) spectrum as a function of the vibrational frequency and contributions of different phonon branches to κ_l for the optimized unit cell of ZrS₂ ML are shown in figure 6. The low energy phonons below 160 cm⁻¹ are found to account for about 91% (94%) of the total κ_l value within BTE (SCP + BTE) method at 300 K. The increase in cumulative κ_l becomes negligible above the phonon frequency of 160 cm⁻¹ indicating the major contribution of the acoustic modes to κ_l . The significant decrease of κ_l values above 160 cm⁻¹ is attributed to the increase in the available three-phonon scattering phase space (SPS), which describes the number of scattering channels available for a phonon. In ZrS₂ ML system, the three-phonon SPS at 300 K increases upon increasing the phonon frequency (above 160 cm⁻¹ as shown in figure S1, Supplemental Material), which corresponds to the subsequently lower κ_l [73,74] thereby increasing the available scattering channels. The three phonon SPS values for absorption processes at 300 K reach to its minimum at higher frequencies (figure S1, Supplemental Material). In contrast, the SPS values for emission processes reach the peak at higher frequencies for both the harmonic and SCP methods. The contribution of different phonon branches to LTC is shown in figure 6(b). The low-energy acoustic phonon modes (branch 1 to 3) are found to have major contributions to the κ_l values than the higher-energy optical modes (branch 4 to 9). In specific, the phonon branch 2 (branch 3) is found to have the highest contribution to κ_l within BTE (SCP + BTE) approach.

Figure 7 shows the temperature dependence of LTC (κ_l) values of the DFT optimized unit cell of ZrS₂ ML calculated by using the conventional BTE and SCP + BTE approaches. The LTC calculations were performed using a sufficiently high $60 \times 60 \times 1$ q -grid points with the neighboring images separated by a sufficiently large vacuum of 22 Å in the z -direction for both the BTE and SCP + BTE methods. The value of κ_l is found to decrease with increasing temperature, in line with the standard relation $\kappa_l \propto T^{-1}$. This behavior is ascribed to the increase in the phonon linewidth (Γ_q^{anh}) (see figure S2, Supplemental Material) at higher temperatures, which is simply related to the increase in the BE distribution function with the temperature that leads to an increase in the scattering probability. The anisotropy in LTC values between the zigzag and armchair directions is appreciably enhanced within the SCP + BTE approach as illustrated in figure 7, which is attributed to the increase in the lattice anharmonicity upon the inclusion of the quartic IFCs. The calculated average κ_l value of ZrS₂ ML at 300 K using the BTE method is 3.19 Wm⁻¹K⁻¹ (3.16 Wm⁻¹K⁻¹ along zigzag direction and 3.22 Wm⁻¹K⁻¹ along armchair direction), which is in agreement with the recently reported result of 3.29 Wm⁻¹K⁻¹ [21] obtained within the BTE method. The predicted κ_l value of ZrS₂ ML in this work is found to be lower than that of bulk ZrS₂ along the in-plane direction, but higher as compared to that along the cross-plane direction [72], see table 2. It is remarkable that the calculated κ_l values by SCP + BTE method are found to be relatively higher than those obtained by the conventional BTE method. At 300K, the average κ_l value of ZrS₂ ML by using SCP + BTE approach is found to be 3.85 Wm⁻¹K⁻¹ (4.28 Wm⁻¹K⁻¹ along zigzag direction and 3.39 Wm⁻¹K⁻¹ along armchair direction), which is higher than the BTE value by 21%. A deeper insight into the origin of the difference in κ_l can be obtained by comparing the calculated phonon linewidth (Γ_q^{anh}) within the BTE and SCP + BTE approaches (see figure S2, Supplemental Material), where $\kappa_l \propto (\Gamma_q^{anh})^{-1}$ as discussed above. The lower value of Γ_q^{anh} within SCP + BTE approach (which uses SCP lattice dynamics) than that within the BTE approach (which uses harmonic lattice dynamics) leads to a higher LTC value for the SCP + BTE approach ($\kappa_l^{SCP+BTE} > \kappa_l^{BTE}$). These outcomes are in line with previous studies [15,31,42] that predicted the anharmonic lattice dynamics properties of cubic SrTiO₃ and SCF₃ using SCP + BTE approach, where the calculated results using SCP + BTE approach were found to agree well with the experimental results. Most crucially, the usual BTE approach neglects the temperature dependence of the phonon frequencies as it takes only the harmonic phonon frequencies into account. With these all facts, the κ_l value calculated using the SCP + BTE approach is expected to be more

accurate, and helps to predict reliable TE figure of merit value and energy conversion efficiency. The prediction should be validated by a future experimental study.

5. Conclusion

The lattice dynamical properties of 2D ZrS₂ ML are investigated using the SCP theory. The CSLD technique has proven to be a useful approach, as an alternative of the computationally expensive DFT calculations, to estimate the higher order anharmonic IFCs. The temperature-dependent phonon frequencies renormalized with the quartic anharmonicity are calculated nonperturbatively based on the SCP approach. The frequency renormalization phenomenon is found to be more pronounced at the low-energy optical modes. The LTC value obtained using the SCP + BTE approach is enhanced as compared to that predicted using the conventional BTE method. This is attributed to the relatively lower phonon linewidth due to the anharmonic phonon frequency renormalization phenomena included within the SCP theory. The conventional BTE approach i) neglects the temperature dependence of the phonon frequencies due to the consideration of harmonic lattice dynamics and ii) the normal process of three-phonon scattering is incorrectly treated due to the use of quasi-particle lifetimes. These limitations are addressed in this work within the SCP + BTE approach, which indicate the validity and accuracy of the approach. We expect that the present work not only correct the κ_l value of ZrS₂ ML reported previously but also provides an insight to explain the effect of phonon anharmonicity on the lattice dynamics and thermodynamic properties. The effect of anharmonic frequency renormalization on the lattice dynamics of similar ultralow-LTC 2D materials followed by the experimental findings could be interesting future works regarding the TE efficiency measurement and device applications.

Data availability statement

The data that support the findings of this study are available upon reasonable request.

Acknowledgements

A. Pandit thanks T. Tadano for the useful discussions. All calculations were performed through Arkansas High Performance Computing Center at the University of Arkansas.

Supplementary material

Supplementary material for this article is available online at [URL LINK].

Author contributions

A. Pandit performed all the calculations and wrote the manuscript. B. Hamad supervised the work and edited the manuscript.

Conflicts of interest

The authors declare no competing conflict of interest.

References

- [1] Kohn W and Sham L J 1965 Self-Consistent Equations Including Exchange and Correlation Effects *Physical Review* **140** A1133–8
- [2] Fultz B 2010 Vibrational thermodynamics of materials *Progress in Materials Science* **55** 247–352
- [3] Ward A, Broido D A, Stewart D A and Deinzer G 2009 *Ab initio* theory of the lattice thermal conductivity in diamond *Phys. Rev. B* **80** 125203
- [4] Lindsay L, Broido D A and Mingo N 2010 Flexural phonons and thermal transport in graphene *Phys. Rev. B* **82** 115427
- [5] Ashcroft N W and Mermin N D 2021 *Solid state physics*
- [6] Maradudin A A and Fein A E 1962 Scattering of Neutrons by an Anharmonic Crystal *Phys. Rev.* **128** 2589–608
- [7] Gonze X and Vigneron J-P 1989 Density-functional approach to nonlinear-response coefficients of solids *Phys. Rev. B* **39** 13120–8
- [8] Baroni S, Giannozzi P and Testa A 1987 Green's-function approach to linear response in solids *Phys. Rev. Lett.* **58** 1861–4
- [9] Baroni S, de Gironcoli S, Dal Corso A and Giannozzi P 2001 Phonons and related crystal properties from density-functional perturbation theory *Rev. Mod. Phys.* **73** 515–62
- [10] Esfarjani K and Stokes H T 2008 Method to extract anharmonic force constants from first principles calculations *Phys. Rev. B* **77** 144112

- [11] Pawley G S, Cochran W, Cowley R A and Dolling G 1966 Diatomic Ferroelectrics *Phys. Rev. Lett.* **17** 753–5
- [12] Holt M, Zschack P, Hong H, Chou M Y and Chiang T-C 2001 X-Ray Studies of Phonon Softening in TiSe 2 *Phys. Rev. Lett.* **86** 3799–802
- [13] Delaire O, Ma J, Marty K, May A F, McGuire M A, Du M-H, Singh D J, Podlesnyak A, Ehlers G, Lumsden M D and Sales B C 2011 Giant anharmonic phonon scattering in PbTe *Nature Mater* **10** 614–9
- [14] Ghosez P Sc H, Gonze X and Michenaud J P 1998 AB initio phonon dispersion curves and interatomic force constants of barium titanate *Ferroelectrics* **206** 205–17
- [15] Tadano T and Tsuneyuki S 2015 Self-consistent phonon calculations of lattice dynamical properties in cubic SrTiO 3 with first-principles anharmonic force constants *Phys. Rev. B* **92** 054301
- [16] Rousseau B and Bergara A 2010 Giant anharmonicity suppresses superconductivity in AlH 3 under pressure *Phys. Rev. B* **82** 104504
- [17] Errea I, Calandra M and Mauri F 2013 First-Principles Theory of Anharmonicity and the Inverse Isotope Effect in Superconducting Palladium-Hydride Compounds *Phys. Rev. Lett.* **111** 177002
- [18] Errea I, Calandra M and Mauri F 2014 Anharmonic free energies and phonon dispersions from the stochastic self-consistent harmonic approximation: Application to platinum and palladium hydrides *Phys. Rev. B* **89** 064302
- [19] Errea I, Calandra M, Pickard C J, Nelson J, Needs R J, Li Y, Liu H, Zhang Y, Ma Y and Mauri F 2015 High-Pressure Hydrogen Sulfide from First Principles: A Strongly Anharmonic Phonon-Mediated Superconductor *Phys. Rev. Lett.* **114** 157004
- [20] Zhao L-D, Lo S-H, Zhang Y, Sun H, Tan G, Uher C, Wolverton C, Druvid V P and Kanatzidis M G 2014 Ultralow thermal conductivity and high thermoelectric figure of merit in SnSe crystals *Nature* **508** 373–7
- [21] Lv H Y, Lu W J, Shao D F, Lu H Y and Sun Y P 2016 Strain-induced enhancement in the thermoelectric performance of a ZrS 2 monolayer *J. Mater. Chem. C* **4** 4538–45
- [22] Kojima A, Teshima K, Shirai Y and Miyasaka T 2009 Organometal Halide Perovskites as Visible-Light Sensitizers for Photovoltaic Cells *J. Am. Chem. Soc.* **131** 6050–1
- [23] Frost J M and Walsh A 2016 What Is Moving in Hybrid Halide Perovskite Solar Cells? *Acc. Chem. Res.* **49** 528–35

- [24] Gunder A S, Paillard C, Pandit A, Haleoot R, Bellaiche L and Hamad B 2021 Effect of the polar distortion on the thermoelectric properties of GeTe *Eur. Phys. J. B* **94** 11
- [25] Wang C Z, Chan C T and Ho K M 1990 Tight-binding molecular-dynamics study of phonon anharmonic effects in silicon and diamond *Phys. Rev. B* **42** 11276–83
- [26] de Koker N 2009 Thermal Conductivity of MgO Periclase from Equilibrium First Principles Molecular Dynamics *Phys. Rev. Lett.* **103** 125902
- [27] Zhang D-B, Sun T and Wentzcovitch R M 2014 Phonon Quasiparticles and Anharmonic Free Energy in Complex Systems *Phys. Rev. Lett.* **112** 058501
- [28] Bianco R, Errea I, Paulatto L, Calandra M and Mauri F 2017 Second-order structural phase transitions, free energy curvature, and temperature-dependent anharmonic phonons in the self-consistent harmonic approximation: Theory and stochastic implementation *Phys. Rev. B* **96** 014111
- [29] Hellman O, Abrikosov I A and Simak S I 2011 Lattice dynamics of anharmonic solids from first principles *Phys. Rev. B* **84** 180301
- [30] Werthamer N R 1970 Self-Consistent Phonon Formulation of Anharmonic Lattice Dynamics *Phys. Rev. B* **1** 572–81
- [31] Tadano T and Tsuneyuki S 2018 First-Principles Lattice Dynamics Method for Strongly Anharmonic Crystals *J. Phys. Soc. Jpn.* **87** 041015
- [32] Zhou F, Nielson W, Xia Y and Ozoliņš V 2014 Lattice Anharmonicity and Thermal Conductivity from Compressive Sensing of First-Principles Calculations *Phys. Rev. Lett.* **113** 185501
- [33] Zeng Z, Yin Z, Huang X, Li H, He Q, Lu G, Boey F and Zhang H 2011 Single-Layer Semiconducting Nanosheets: High-Yield Preparation and Device Fabrication *Angew. Chem. Int. Ed.* **50** 11093–7
- [34] Zhang M, Zhu Y, Wang X, Feng Q, Qiao S, Wen W, Chen Y, Cui M, Zhang J, Cai C and Xie L 2015 Controlled Synthesis of ZrS₂ Monolayer and Few Layers on Hexagonal Boron Nitride *J. Am. Chem. Soc.* **137** 7051–4
- [35] Mañas-Valero S, García-López V, Cantarero A and Galbiati M 2016 Raman Spectra of ZrS₂ and ZrSe₂ from Bulk to Atomically Thin Layers *Applied Sciences* **6** 264
- [36] Herninda T M and Ho C-H 2020 Optical and Thermoelectric Properties of Surface-Oxidation Sensitive Layered Zirconium Dichalcogenides ZrS₂-xSex (x = 0, 1, 2) Crystals Grown by Chemical Vapor Transport *Crystals* **10** 327

- [37] Qin G, Qin Z, Fang W-Z, Zhang L-C, Yue S-Y, Yan Q-B, Hu M and Su G 2016 Diverse anisotropy of phonon transport in two-dimensional group IV–VI compounds: A comparative study *Nanoscale* **8** 11306–19
- [38] Shafique A and Shin Y-H 2017 Thermoelectric and phonon transport properties of two-dimensional IV–VI compounds *Sci Rep* **7** 506
- [39] Dong B, Wang Z, Hung N T, Oganov A R, Yang T, Saito R and Zhang Z 2019 New two-dimensional phase of tin chalcogenides: Candidates for high-performance thermoelectric materials *Phys. Rev. Materials* **3** 013405
- [40] Pandit A and Hamad B 2021 Thermoelectric and lattice dynamics properties of layered MX (M = Sn, Pb; X = S, Te) compounds *Applied Surface Science* **538** 147911
- [41] Pandit A, Haleoot R and Hamad B 2020 Thermal conductivity and enhanced thermoelectric performance of SnTe bilayer *arXiv:2006.16410 [cond-mat]*
- [42] Tadano T and Tsuneyuki S 2018 Quartic Anharmonicity of Rattlers and Its Effect on Lattice Thermal Conductivity of Clathrates from First Principles *Phys. Rev. Lett.* **120** 105901
- [43] Oba Y, Tadano T, Akashi R and Tsuneyuki S 2019 First-principles study of phonon anharmonicity and negative thermal expansion in ScF₃ *Phys. Rev. Materials* **3** 033601
- [44] Paulatto L, Errea I, Calandra M and Mauri F 2015 First-principles calculations of phonon frequencies, lifetimes, and spectral functions from weak to strong anharmonicity: The example of palladium hydrides *Phys. Rev. B* **91** 054304
- [45] Kato T 1995 *Perturbation Theory for Linear Operators* vol 132 (Berlin, Heidelberg: Springer Berlin Heidelberg)
- [46] Zeng Z, Li S, Tadano T and Chen Y 2020 Anharmonic lattice dynamics and thermal transport of monolayer InSe under equibiaxial tensile strains *J. Phys.: Condens. Matter* **32** 475702
- [47] Hooton D J 1958 The use of a model in anharmonic lattice dynamics *Philosophical Magazine* **3** 49–54
- [48] Koehler T R 1966 Theory of the Self-Consistent Harmonic Approximation with Application to Solid Neon *Phys. Rev. Lett.* **17** 89–91
- [49] Horner H 1967 Lattice dynamics of quantum crystals *Z. Physik* **205** 72–89
- [50] Kresse G and Furthmüller J 1996 Efficiency of ab-initio total energy calculations for metals and semiconductors using a plane-wave basis set *Computational Materials Science* **6** 15–50

- [51] Kresse G and Furthmüller J 1996 Efficient iterative schemes for *ab initio* total-energy calculations using a plane-wave basis set *Physical Review B* **54** 11169–86
- [52] Perdew J P, Burke K and Ernzerhof M 1996 Generalized Gradient Approximation Made Simple *Physical Review Letters* **77** 3865–8
- [53] Klimeš J, Bowler D R and Michaelides A 2011 Van der Waals density functionals applied to solids *Phys. Rev. B* **83** 195131
- [54] Tadano T, Gohda Y and Tsuneyuki S 2014 Anharmonic force constants extracted from first-principles molecular dynamics: applications to heat transfer simulations *J. Phys.: Condens. Matter* **26** 225402
- [55] Hastie T, Friedman J H and Tibshirani R *The Elements of Statistical Learning: Data Mining, Inference, and Prediction*
- [56] Li W, Carrete J, A. Katcho N and Mingo N 2014 ShengBTE: A solver of the Boltzmann transport equation for phonons *Computer Physics Communications* **185** 1747–58
- [57] Gu X and Yang R 2014 Phonon transport in single-layer transition metal dichalcogenides: A first-principles study *Appl. Phys. Lett.* **105** 131903
- [58] Mounet N, Gibertini M, Schwaller P, Campi D, Merkys A, Marrazzo A, Sohier T, Castelli I E, Cepellotti A, Pizzi G and Marzari N 2018 Two-dimensional materials from high-throughput computational exfoliation of experimentally known compounds *Nature Nanotech* **13** 246–52
- [59] Oliver S M, Fox J J, Hashemi A, Singh A, Cavalero R L, Yee S, Snyder D W, Jaramillo R, Komsa H-P and Vora P M 2020 Phonons and excitons in ZrSe_2 – ZrS_2 alloys *J. Mater. Chem. C* **8** 5732–43
- [60] Shang J, Zhang S, Cheng X, Wei Z and Li J 2017 Electric field induced electronic properties modification of ZrS_2 / HfS_2 van der Waals heterostructure *RSC Adv.* **7** 14625–30
- [61] Özbal G, Senger R T, Sevik C and Sevinçli H 2019 Ballistic thermoelectric properties of monolayer semiconducting transition metal dichalcogenides and oxides *Phys. Rev. B* **100** 085415
- [62] Castro Neto A H, Guinea F, Peres N M R, Novoselov K S and Geim A K 2009 The electronic properties of graphene *Rev. Mod. Phys.* **81** 109–62
- [63] Kagdada H L, Jha P K, Śpiewak P and Kurzydłowski K J 2018 Understanding the behavior of electronic and phonon transports in germanium based two dimensional chalcogenides *Journal of Applied Physics* **124** 235701

- [64] Gupta S K, Soni H R and Jha P K 2013 Electronic and phonon bandstructures of pristine few layer and metal doped graphene using first principles calculations *AIP Advances* **3** 032117
- [65] Koukaras E N, Kalosakas G, Galiotis C and Papagelis K 2015 Phonon properties of graphene derived from molecular dynamics simulations *Sci Rep* **5** 12923
- [66] D'Souza R and Mukherjee S 2017 Length-dependent lattice thermal conductivity of single-layer and multilayer hexagonal boron nitride: A first-principles study using the Callaway-Klemens and real-space supercell methods *Phys. Rev. B* **96** 205422
- [67] Jha P K and Soni H R 2014 Strain induced modification in phonon dispersion curves of monolayer boron pnictides *Journal of Applied Physics* **115** 023509
- [68] Xie H, Ouyang T, Germaneau É, Qin G, Hu M and Bao H 2016 Large tunability of lattice thermal conductivity of monolayer silicene via mechanical strain *Phys. Rev. B* **93** 075404
- [69] Shafique A and Shin Y-H 2020 The effect of non-analytical corrections on the phononic thermal transport in InX (X = S, Se, Te) monolayers *Sci Rep* **10** 1093
- [70] Cai Y, Lan J, Zhang G and Zhang Y-W 2014 Lattice vibrational modes and phonon thermal conductivity of monolayer MoS₂ *Phys. Rev. B* **89** 035438
- [71] Ziman J M 2001 *Electrons and phonons: the theory of transport phenomena in solids* (Oxford : New York: Clarendon Press ; Oxford University Press)
- [72] Glebko N and Karttunen A J 2019 Lattice thermal conductivity of TiS₂, ZrS₂, and HfS₂: Periodic trends studied by dispersion-corrected hybrid density functional methods *Phys. Rev. B* **100** 024301
- [73] Lindsay L and Broido D A 2008 Three-phonon phase space and lattice thermal conductivity in semiconductors *J. Phys.: Condens. Matter* **20** 165209
- [74] Malakkal L, Prasad A, Oladimeji D, Jossou E, Ranasinghe J, Szpunar B, Bichler L and Szpunar J 2019 Atomistic and experimental study on thermal conductivity of bulk and porous cerium dioxide *Sci Rep* **9** 6326

FIGURES

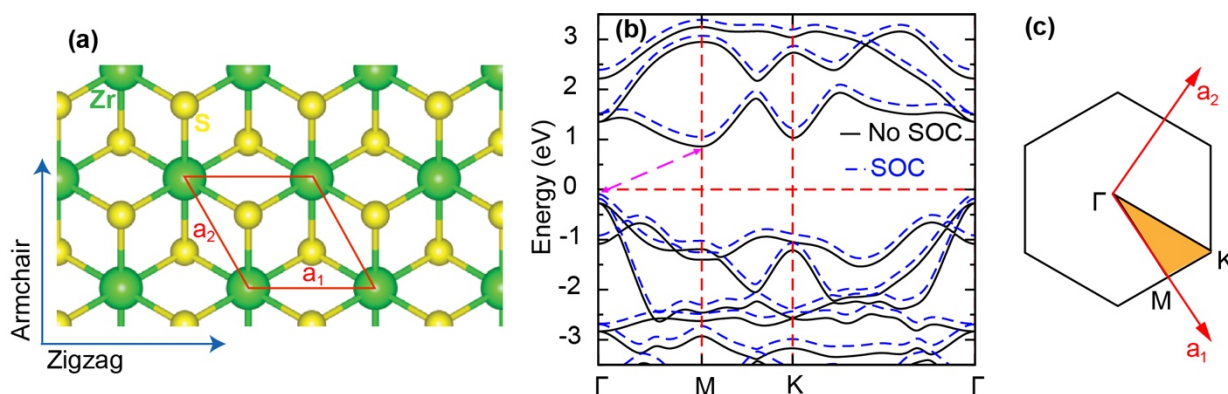


Figure 1. (Color online) (a) Crystal structure of ZrS_2 ML, the red rhombic box denotes the primitive unit cell. (b) The electronic band structure of ZrS_2 ML along the high-symmetry path $\Gamma - \text{M} - \text{K} - \Gamma$ in the first Brillouin zone, the solid and dotted lines indicate the bands without and with spin-orbit interaction, respectively. (c) The Brillouin zone with labelled high-symmetry points.

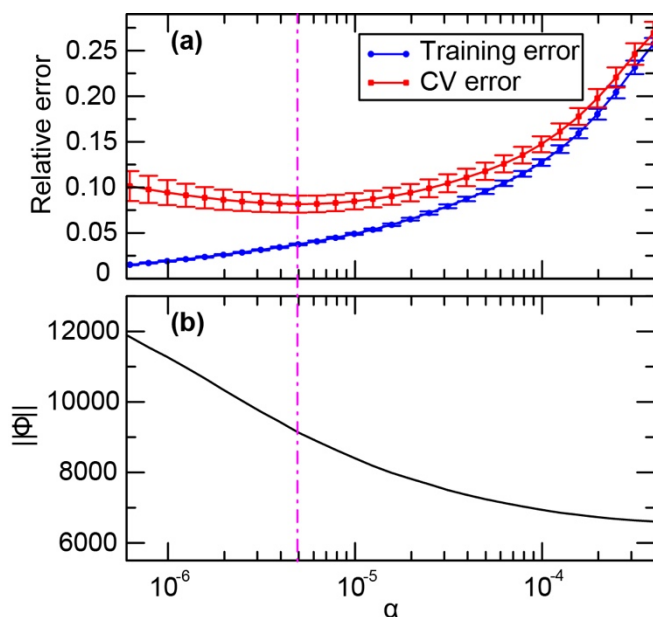


Figure 2. (Color online) (a) Relative errors in the atomic forces and (b) the number of non-zero quartic IFCs as a function of the hyperparameter (α). The dotted vertical line represents the value of α at which the cross-validation error is minimum.

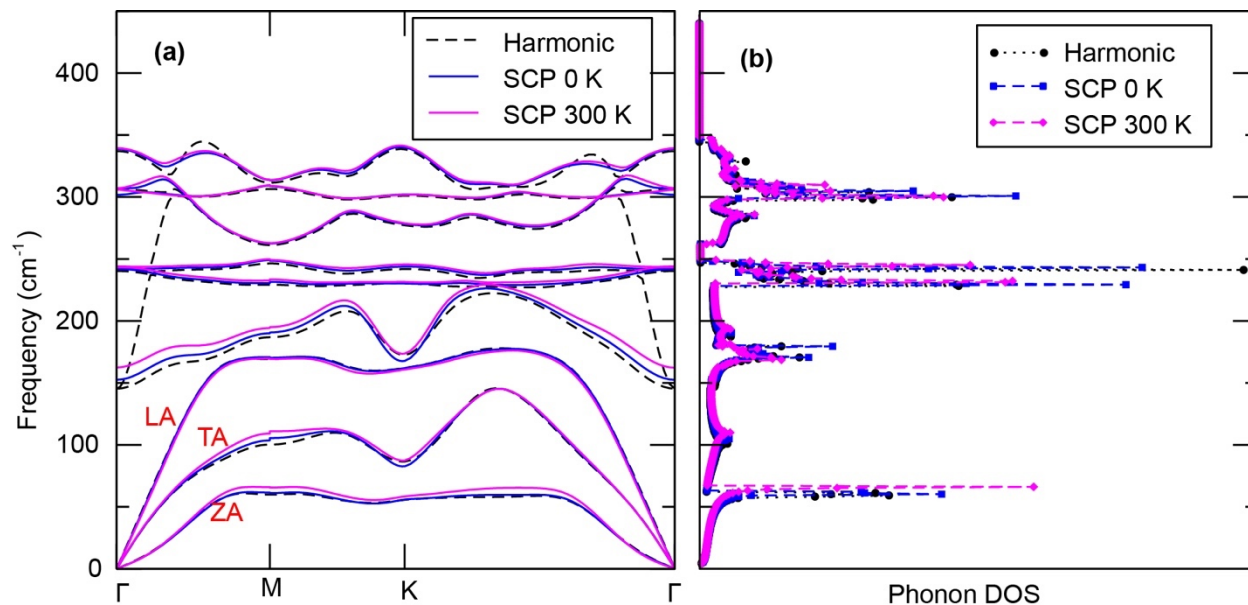


Figure 3. (Color online) (a) Temperature-dependent anharmonic phonon dispersion and (b) the phonon density of states (DOS) of the ZrS_2 ML. The black dotted lines indicate the harmonic lattice dynamics.

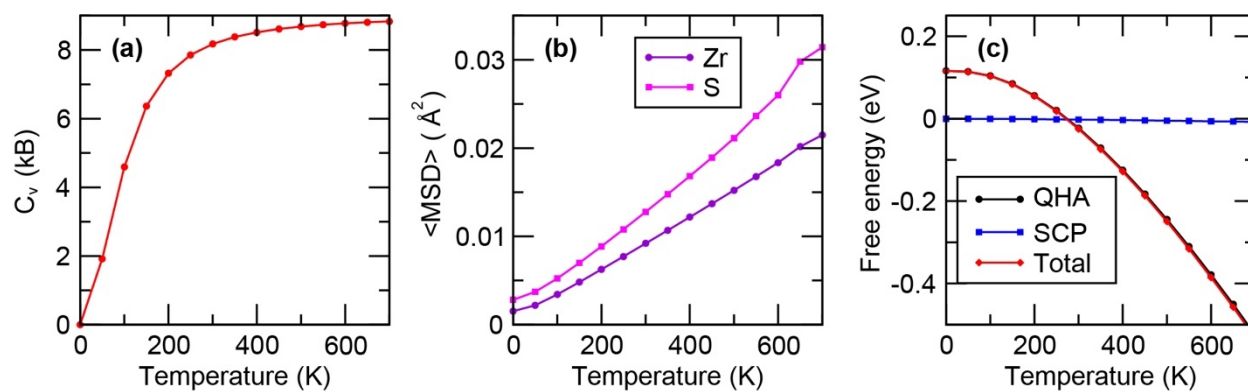


Figure 4. (Color online) Temperature dependence of (a) the specific heat capacity and (b) the root mean-square displacement of the Zr and S atoms, and (c) free energies within the QHA and SCP correction for the ZrS_2 ML.

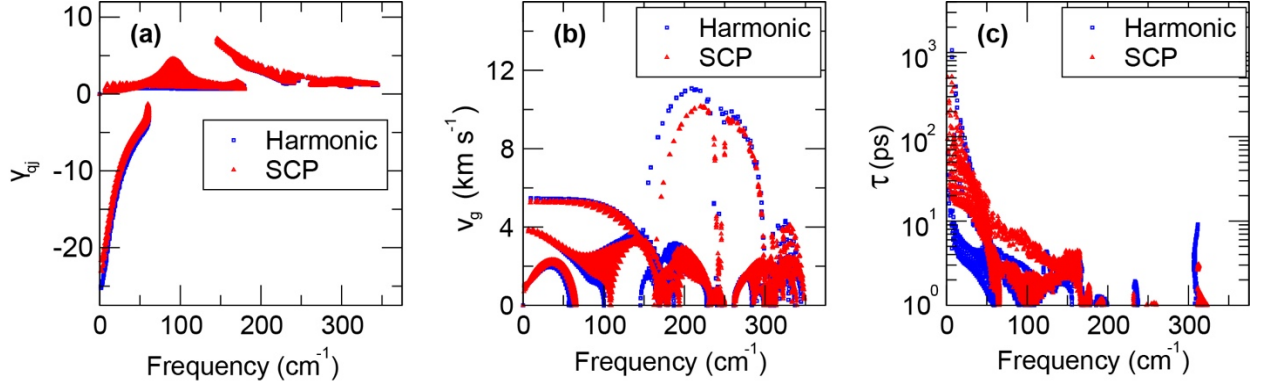


Figure 5. (Color online) (a) Grüneisen parameter, (b) the cumulative phonon group velocity, and (c) the phonon lifetime of ZrS₂ ML as a function of the phonon vibrational frequency obtained with the harmonic and SCP lattice dynamics.

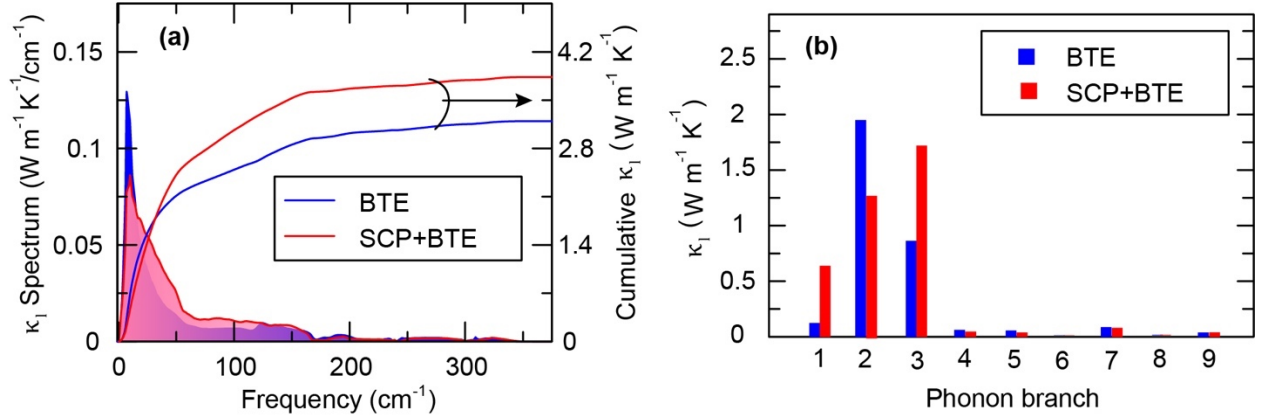


Figure 6. (Color online) (a) LTC (κ_l) spectrum and cumulative κ_l as a function of the phonon frequency and (b) contributions of different phonon branches to the LTC of 2D ZrS₂ ML at 300 K obtained with the BTE and SCP + BTE methods. In (a), the curves with shaded region indicate the κ_l spectrum and the curves without shade indicate cumulative κ_l .

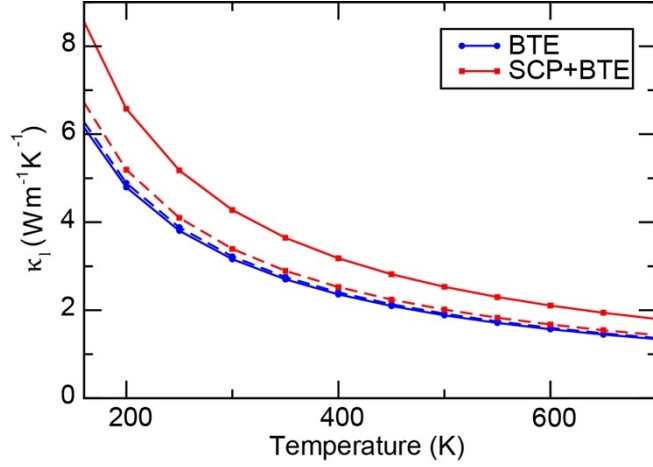


Figure 7. (Color online) LTC (κ_l) of the ZrS₂ ML as a function of temperature obtained with the BTE and SCP + BTE approach. The solid and dotted lines indicate the values along zigzag and armchair directions, respectively.

TABLES

Table 1. Phonon frequencies (cm⁻¹) of the lower optical modes of ZrS₂ ML calculated using different approaches.

Phonon modes	Harmonic	SCP at 0 K	SCP at 300 K
4	145.36	152.57	162.55
5	145.38	230.55	243.45

Table 2. Calculated LTC of 2D ZrS₂ ML and its bulk system at 300 K.

System	κ_l (Wm ⁻¹ K ⁻¹) at 300 K	References
ZrS ₂ ML	3.19	This work (BTE)
	3.85	This work (SCP + BTE)
	3.29	Previous work (BTE) [21]
ZrS ₂ Bulk	8.5 (In plane)	Previous work (BTE) [72]
	1.4 (Cross plane)	